Interaction of superconducting $YBa_2Cu_{3-x}Zn_xO_{7-y}$ with MeV radiation

R.A. Lewis*
RLewis Company, Boalsburg, PA 16827

G. A. Robertson†
Marshall Space Flight Center, Huntsville, Alabama 35812
(Dated: March 17, 2005)

When the high Tc superconductor Y-Ba-Cu-O is cooled with liquid nitrogen, the conduction holes form a macroscopic collective or entangled state. While collective effects have been observed with radiation energies up to 5 eV, no high-sensitivity experiments have previously been carried out to search for comparable effects with MeV radiation. Here an experiment using a pair of scintillation counters arranged to search for changes in the natural background of high energy radiation adjacent to a warm and cold Y-Ba-Cu-O superconductor is described. The experiment showed a shift toward higher pulse heights when the SC was cooled, with a 4 standard deviation excess of 9.12±2.28 events/ksec over the range of 0 to 18 MeV. The net difference spectrum shows a 5.5 standard deviation excess signal for the range of 3 to 6 MeV.

PACS numbers: 07.85.-m, 13.85.Rm, 87.56.By, 29.25.Rm, 74.

Phase transitions in a superconductor (SC) involve the creation and destruction of a scalar field[1], associated with a collective or entangled state involving many particles. The effects associated with superconductivity are identified by comparing results with warm and cold SC. Superconductor collective effects have been observed during interactions with ultraviolet[2] and neutron[3] radiation at low (eV) energy levels. Here the properties of a superconductor are explored with MeV radiation from the natural background. Flux pinning is utilized, since tests of radiation interactions might be more sensitive to effects of the quantized vortices[4] present in a flux pinned superconductor. The experiment was arranged to measure horizontal radiation, to suppress the high rate of background from vertical cosmic rays.

For the tests, two Bicron model BC-408, polyvinyltoluene scintillators with paddle dimensions of 1/4" x 2.75" x 11" attached to an ETI 9266 photomultiplier tube (PMT) were chosen. The BC-408 scintillation counter can detect any kind of radiation which can get through the paper wrapping, and cause ionization in the plastic material. For example, MeV gamma rays have a 3% probability for producing ionization by Compton scattering in 1/4" of plastic scintillator. The two scintillation counters were placed approximately 6" apart and between the SC cooldown position and warmup position as shown in FIG. 1. The SC was cooled with liquid nitrogen (LN2) in a small container. The LN2 container was composed of 1/8" circuit board material soldered together in an open box fashion and surrounded by Styrofoam for insulation (using RTV and black duct tape). The LN2 container was made, such that, two stacked 2" square by 1/2" thick NdFeB magnets could be placed under and directly against the circuit board material for flux pinning in the SC. The magnetic field strength at the bottom center of the LN2 container was measured to be 3.5 kG. The magnetic shielding around the PMT's was augmented by two layers of μ-metal, to make the counters insensitive to the NdFeB magnet. Before the μ-metal shields were applied, the sensitivity of the nearest counter decreased by 3% when the NdFeB magnet was moved into place. The decrease in count rate from a Co^{60} source was equivalent to attenuating the PMT signal by 3%, determined using Joerger QVSC scalers and a Pasternack ENT variable attenuator. Pulse heights changed by less than 1.1% when the μ-metal shield was present.

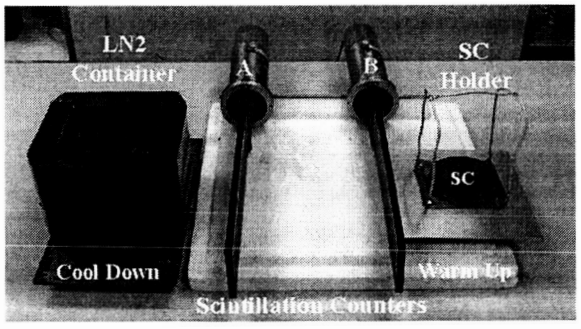

FIG. 1: Layout of scintillation counters, YBaCuO superconductor (SC), Cool Down LN2 Container, and SC holder on warming Plate.

The photomultiplier signals from the two scintillation counters were divided using three 16 Ω resistors to provide a balanced separation of the signals. One pair of the signals was amplified by one stage of a Stanford Research Systems 240 preamp, which provides a gain of 5 (14 dB). These signals were digitized using LeCroy 623 discriminators, set to a threshold of 40 mV and a width of 60 ns and sent to a LeCroy 365 logic unit to determine coincidences. The second pair was amplified by Ortec FTA-820 fast amps (nominal gain of 200) and sent to either a Tektronix TDS-7104 digital oscilloscope for preliminary timing adjustments or to a National Instrument PXI-5112 high-speed digitizer embedded in a PXI-1010 chassis with an embedded PXI-5156B pentium base con-

troller for data collection. The output of the LeCroy 365 logic unit was used as the trigger for the high-speed digitizer. A LabView (version 7.0) program was written to integrate the signals received by the PXI-5112 high-speed digitizer. The integrated signals were plotted and saved to a file.

The scintillation counters were calibrated using a vertical arrangement to detect cosmic rays. The gains on the two counters were equalized, so that the average of the two pulse heights is proportional to the energy deposited. A typical pulse height spectrum, FIG. 2, shows a peak corresponding to single charged particles, the Landau tail, and a low-energy continuum attributable to gamma rays. On average, cosmic ray muons deposit[5] 3.2 MeV of energy in two 1/4" thick counters, implying a calibration of 2.2 MeV/volt. The cutoff at 0.3 volts corresponds to 0.66 MeV.

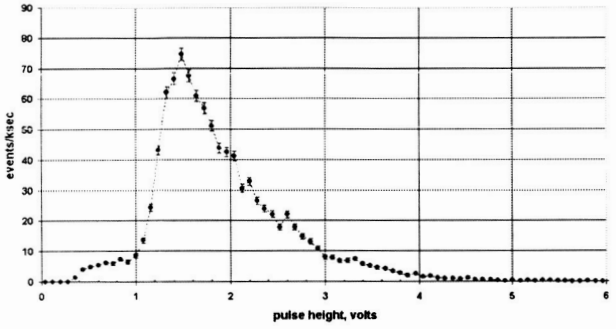

FIG. 2: Pulse Height distribution from cosmic rays.

A top seeded, melt growth process SC disk with diameter of 4" and total thickness of 0.6" was chosen for the SC test runs as it exhibited very strong flux pinning characteristics. This SC contains two layers of approximately equal thicknesses, with different compositions as the interface between the two layers is very distinctive and partially separated. SEM analysis showed both layers to be composed of Yttrium (Y), Barium (Ba), Copper (Cu), Oxygen (O), and a small amount of Zinc (Zn). Zinc is one of several additives used to enhance the flux pinning properties of the Y-Ba-Cu-O (YBCO) SC[6]. The top layer is denser than the bottom and has seven top-seeded large crystal growth sites[7]. The crystal growth is very large, on the order of 1" in a hex pattern as shown in Fig. 3. Each top-seeded site behaved like a single magnet when flux was pinned in the SC, as was evidenced by a small magnet being attracted to and levitated over each seed site. A SEM analysis was conducted on small samples taken from the outer edge of the SC to determine its material composition. The conclusion from the SEM analysis and visual inspection of the SC is that the top layer is composed of $YBa_2Cu_{3-x}Zn_xO_{7-y}$ using the top-seeded, melt-growth process, where zinc and top-seeding is used to enhance the flux pinning properties of the YBCO SC[8]. The bottom layer is possibly a side effect of the top-seeded melt growth process where the green $Y_2Ba_1Cu_1O$ phase is commonly used as a base to prevent unwanted reactions with the substrate.

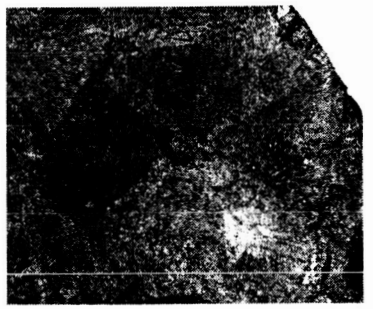

FIG. 3: One of seven large single crystal sites on top of the YBCO + Zn SC disk.

In a typical run, the SC was placed into the LN2 container near scintillation counter A, lowering its temperature below its critical temperature ($\sim$ 90 K). Preliminary measurements with no pinning magnet indicated that this took $\sim$ 5 minutes, as judged by a magnet placed over the SC and from the LN2 boil off about the SC. Once the SC was cooled, it was removed from the LN2 container and placed on an aluminum plate near scintillation counter B and allowed to warm up. Warmup times were judged by the melting of the ice, which formed on the SC. Typical warmup times were 15-20 minutes. However, preliminary tests with a small magnet indicated that the superconductive levitation properties were gone within 5-6 minutes.

Increases in the pinning magnetic field were measured during cooldown tests with no SC present. As noted, the magnetic field 10 cm from the NdFeB magnet increases from 98 to 103 Gauss when LN2 is transferred to the container. Measurements of the pinned magnetic field 10 cm from the cold SC with the pinning magnet removed was measured to be 3 Gauss. The magnetic fields should have only a minor effect on MeV radiation, since the cyclotron radius of electrons is large compared with dimensions of the apparatus.

Event rates varied from 138.2±3.6 events/ksec during cooldown/warmup runs compared to 128.7±1.6 events/ksec during background runs. Background runs were conducted with the SC on the aluminum plate at room temperature, using the same geometry as for the warmup portion of cooldown/warmup tests. Energy-weighted pulse height distributions from a set of 16 cooldown/warmup runs and two background runs are shown in FIG. 4.

The pulse height spectrum from the SC runs follows the general shape of the background runs. The rates for signals from the cold SC between 2 and 3 MeV are systematically 20% lower than the background. In the 3-6 MeV range, radiation from the cold SC produced a higher rate of pulses. The average energies from integrals of the spectra are listed in TABLE I.

More information on the possible mechanism for the

TABLE I: Average Energy Values.

SC Runs:
$545.39 \pm 9.09\ MeV/ksec$

Background Runs:
$504.33 \pm 4.75\ MeV/ksec$

Net signal:
$= 41.06 \pm 10.26\ MeV/ksec$
$39.09 \pm 6.98\ MeV/ksec$ (3.168 to 5.808 MeV)
$8.95 \pm 1.64\ events/ksec$ (3.168 to 5.808 MeV)

difference in pulse height spectra is obtained by subtracting the two spectra bin by bin as shown in FIG. 5. The net difference spectrum shows a systematic enhancement for energies of 3 to 6 MeV, indicating a 5.5 standard deviation in this range. Pulse heights in this energy range are consistent with energy deposition by 2 to 4 relativistic particles. A likely mechanism is that the counters pick up the initial stages of electromagnetic showers. That is, the counters are too thin to absorb a major fraction of the shower energy.

The dearth of signals with 2 to 3 MeV pulse heights is statistically significant. The dearth could possibly be explained if the counters were 3% more sensitive during cold SC runs than during background runs. Attempting to ascribe the 3% shift as variations in energy deposition dE/dx would require a model of the energy spectrum of horizontal radiation. The measured rate of 0.13 events/second is several orders of magnitude higher than the flux of horizontal cosmic rays , implying that the background is mostly due to secondary interactions of cosmic rays.

Pulse heights from the PXI-5112 digitizers are quantized in units of 13.7 mV. The bin widths correspond to 160 mV for the sum of A and B pulse heights, or an average of $160/13.7 = 11.7$ quanta per bin. Individual bins can encompass either 11 or 12 quanta. Quantization can account for ±9% bin-to-bin variations, larger than statistical variations in high-statistics runs. The quantization effects cannot explain 12 high bins in succession observed in the data as shown in FIG. 5.

Also, the solid angle subtended by counter A for a radiation source in the SC is $(3.0 \pm 0.3)\%$ of 4π steradians, depending on whether the SC is located ±1 cm from the center of the warming plate. High statistics runs are needed to discern any effect due to the SC. For example removing the SC, warmup plate and LN2 container results in a 10% reduction in background rate. For definiteness, suppose that the SC contributes 10% to the background. Then the uncertainty of ±10% in the solid angle of the SC would correspond to a change of ±1% in the background rate. For comparison, table I implies that the ratio of yields with cold and warm superconductor is $R = 545.39/504.33 = 1.081 \pm 0.019$. The 1% possible effect of geometry is small compared with either

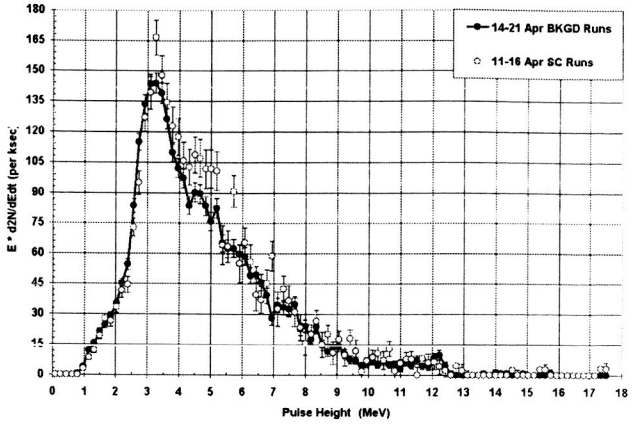

FIG. 4: Energy-weighted spectra for cooldown SC runs, and two background runs.

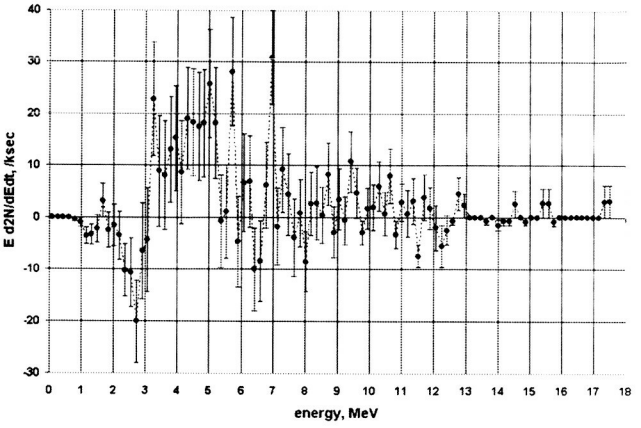

FIG. 5: Subtracted spectra of FIG. 4 shows a 5.5 standard deviation excess signal for 3 to 6 MeV.

the 8.1% increase in rate, or even the 1.9% statistical error. This indicates that the sensitivity of the pulse height spectrum to centimeter variations in the placement of the SC is an order of magnitude below the effects observed with high statistics runs.

To assess systematic effects, the integrated energy was used as a figure of merit and is summarized in FIG. 6. As shown, the SC runs taken during April 11 and 12 (black circles) had durations ranging from 723 to 4089 seconds. To assess whether the excess radiation persisted beyond the 15-20 minute warmup time, the first 180 events of each run were selected (clear circles). Surprisingly, the average detected energy rates were practically the same for the two selections (561.1±10.5 MeV/ksec for all events, 562.5±15.5 MeV/ksec for the first 180 event samples). A fit to the 9 data points of April 11, 12 SC runs resulted in a chi square χ^2 =15.1, which corresponds to a significance level of 6% for 8 degrees of freedom. The variations from run to run are consistent with statistical fluctuations.

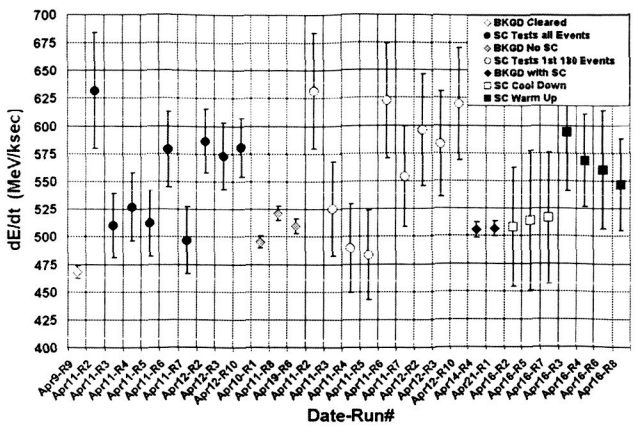

FIG. 6: Run-by-Run summary of detected energy rates.

The diamonds representing room background runs illustrate other features. The background energy spectra differ noticeably depending on the nature of surrounding materials. For example the rate of 467.9±5.80 MeV/ksec with nearby materials removed (clear diamond) is significantly less than 504.33±4.75 MeV/ksec with the warm SC, aluminum plate, LN2 Dewar, and other materials present (black diamonds). For the three background runs, where only the SC was removed (gray diamonds), the average energy rate was 506.9±3.45 MeV/ksec. The χ^2 of 10.1 from fitting the three runs corresponds to a confidence level of 0.6% for two degrees of freedom, suggesting a systematic error of around ±10 MeV/ksec. This indicates that care must be taken to insure that the SC runs and background runs are taken with the same surrounding material conditions. Therefore, for the analysis in this paper, only the background runs with the room temperature SC on the aluminum plate are used for comparison with SC cooldown/warmup runs.

Systematic differences of ±10 MeV/ksec in integrated energy are noted, in three background runs with nominally common conditions. A possible 5% shift in counter gain could explain the lower rate of 2 to 3 MeV signals in SC runs. However no evidence for gain shifts was found by subdividing the background runs into short segments. These systematic effects do not account for the excess of 3 to 6 MeV signals observed during cooldown/warmup runs.

Test runs involving cooldown/warmup of the SC consistently detect a higher rate of radiation than in background runs with a warm present. The net difference is 41.06±10.26 MeV/ksec, or 9.12±2.28 events/ksec in the form of 3 to 6 MeV radiation. Analysis of subsets of the data turned up the surprising feature that the excess radiation persists for nearly an hour during warmup, long after flux pinning is undetectable. This behavior cannot be summarily dismissed, since pairing effects have also been observed in similar superconductors above the critical temperature using magnetization[9] or low-energy neutron scattering[3].

---

* Electronic address: R3L@psu.edu
† Electronic address: glen.a.robertson@nasa.gov

[1] W.H. Zurek, Cosmological experiments in condensed matter systems, Physics Reports **276** (1996) 177-221.
[2] J. Backstrom, D. Budelmann, R. Rauer, and M. Rbhausen, "Optical properties of $YBa_2Cu_3O_{7-d}$ and $PrBa_2Cu_3O_{7-d}$ films: High-energy correlations and metallicity," PHYSICAL REVIEW B **70**, 174502 (2004).
[3] H. F. Fong, P. Bourges, Y. Sidis, L. P. Regnault, J. Bossy, A. Ivanov, D. L. Milius, I. A. Aksay, and B. Keimer, Effect of Nonmagnetic Impurities on the Magnetic Resonance Peak in $YBa_2Cu_3O_7$, Phys. Rev. Lett. **82**, 1939-1942 (1999).
[4] Iwo Bialynicki-Birula, "Particle beams guided by electromagnetic vortices: new solutions of the Lorentz, Schroedinger, Klein-Gordon and Dirac Equations," Phys. Rev. Lett. **93**, 2004.
[5] S. Eidelman et al., Review of particle physics, Physics Letters B **592**, 1, 2004.
[6] T. Strasser, A. Kthler, D. Litzkendorf, K. Fischer, p. Gtrnert, "Modified melt texturing process for YBCO based on the polythermic section $YO_{1.5}Ba_{0.4}Cu_{0.6}$ in the Y-Ba-Cu-O phase diagram at 0.21 bar oxygen pressure," Physica C **244**, pp. 145-152 (1995).
[7] Wai Lo, D. A. Cardwell, and P. D. Hunneyball, "Growth morphology of large YBCO grains fabricated by seeded peritectic solidification: (I) The seeding process," J. Mater. Res., Vol. **13**, No. **8** (1998).
[8] G. Krabbes, G. Fuchs, P. Schatzle, S. Gru, J.W. Park, F. Hardinghaus, G. Stover, R. Hayn, S.-L. Drechsler, T. Fahr, "Zn doping of YBa_2CuO_7 in melt textured materials: peak effect and high trapped fields," Physica C **330**, pp.181-190 (2000).
[9] C. Panagopoulos, M. Majoros and A.P. Petrovic, "Thermal hysteresis in the normal-state magnetization of $La_{2-x}Sr_xCuO_4$," Phys. Rev. B **69**, 144508 (2004).